Mechanism and Machine Theory 101 (2016) 168–180

Contents lists available at ScienceDirect

Mechanism and Machine Theory

journal homepage: www.elsevier.com/locate/mechmt

Analytical compliance analysis and finite element verification of spherical flexure hinges for spatial compliant mechanisms

Farid Parvari Rad[a,*], Rocco Vertechy[a], Giovanni Berselli[b], Vincenzo Parenti-Castelli[a]

[a] Department of Mechanical Engineering, University of Bologna, Italy
[b] Department of Mechanical Engineering, University of Genova, Italy

ARTICLE INFO

Article history:
Received 21 January 2015
Received in revised form 12 January 2016
Accepted 13 January 2016
Available online 7 April 2016

Keywords:
Spherical Flexures
Compliance matrix
Finite Element Analysis
Parasitic motions

ABSTRACT

This paper introduces and investigates a novel Spherical Flexure (SF), specifically conceived for application on spherical compliant mechanisms. The flexure features an arc of a circle as a centroidal axis and an annulus sector as cross-section, circle and annulus having a common center coinciding to that of the desired spherical motion. In this context, each element of the SF spatial compliance matrix is analytically computed as a function of both flexure dimensions and employed material. The theoretical model is then validated by relating analytical data with the results obtained through three-dimensional Finite Element Analysis. Finally, SFs are compared to Circularly Curved-Beam Flexures (CCBFs) in terms of parasitic motions.

1. Introduction

Flexure hinges can profitably substitute traditional kinematic pairs in those articulated mechanisms which require absence of backlash and friction but restricted range of motion. Common applications span high precision manufacturing [1,2], minimally invasive surgery [3,4] and micro-electromechanical systems (MEMS) [5,6]. Several studies have been dedicated to the design, characterization and comparative evaluation of straight-beam flexures and compliant mechanisms formed therewith, see e.g. Refs. [7,8,9]. Lobuntiu and Cullin [10] have recently introduced the two-segment circular-axis symmetric notch flexure and compared its in-plane compliance with that of the straight-axis counterpart. Parvari Rad et al. [11] have evaluated the spatial compliance of Circularly Curved-Beam Flexures (CCBFs), featuring an arc of a circle as a centroidal axis (see curve C in Fig. 1) and a rectangular cross-section (Fig. 2). In addition, Berselli et al. [12] have quantitatively compared CCBFs with straight-beam flexures in terms of maximum achievable rotation and selective compliance.

In any case, most of the aforementioned flexures have been conceived and applied to planar compliant mechanisms. Despite the practical relevance, investigations on compliant hinges specifically designed for spatial mechanisms are instead quite limited. One of the most important classes of spatial mechanisms is the spherical linkage. In spherical mechanisms, all points of the end-link are constrained to move on concentric spherical surfaces that are fixed with respect to the base. To date, only a limited number of works have investigated compliant joints specifically designed for spherical motion, as well as fully compliant spherical mechanisms. Smith [13] proposed compliant universal joints fabricated from circular leaf springs, which also provided axial translation for self-alignment applications. However, the proposed joints are affected by significant stress concentrations that limit their ranges of motion. Lobontiu et al. [14,15] investigated the two- and three-axis flexure hinges. The former consists of

* Corresponding author at: Department of Mechanical Engineering, University of Bologna, Italy. Tel.: +39 051 20 93451, fax: +39 051 20 93446.
E-mail addresses: farid.parvarirad2@unibo.it (F. Parvari Rad), rocco.vertechy@unibo.it (G. Berselli), giovanni.berselli@unige.it (R. Vertechy), vincenzo.parenti@unibo.it (V. Parenti-Castelli).

http://dx.doi.org/10.1016/j.mechmachtheory.2016.01.010
0094-114X/

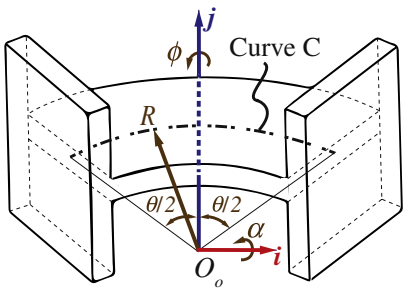

Fig. 1. Circularly curved-beam flexures.

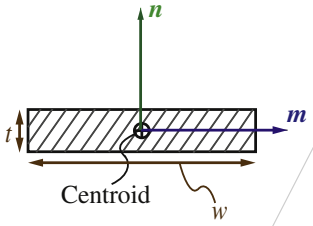

Fig. 2. Cross section properties of CCBFs.

two collocated notches that are cut perpendicular to each other; the latter consists of an axial-symmetric notch. In both cases, the resulting hinge features a small cross-sectional area and is prone to unintentional rotations or buckling even when loaded with small forces. Moon et al. [16] developed a compliant revolute hinge based on torsion beams of cross or segmented-cross type, and employed two of them, connected in series with orthogonal axes, to conceive a fully compliant universal joint. Later on, the ensemble of two universal joints of this kind has been proposed by Machekposhti et al. [17] to obtain a compliant constant velocity Double-Hooke's universal joint. Different authors [18,19] employed two in-series connected flexure notch hinges with orthogonal axes to conceive a fully compliant universal joint. Jacobsen et al. [20] employed three in-series connected lamina emergent torsional joints, with axes intersecting in a single point, to make spherical chains with three degrees of freedom (for compliant joints or mechanisms, the number of degrees of freedom is intended as the number of independent prevalent directions of motion). These spherical chains were then used to build a 3-RRR spherical parallel mechanism (R being a revolute joint). Callegari et al. [21] addressed the analysis and design of a 3-CRU spherical parallel mechanism with flexure hinges (C and U being cylindrical and universal joints respectively). Li and Chen [22] employed two circularly curved deformable segments

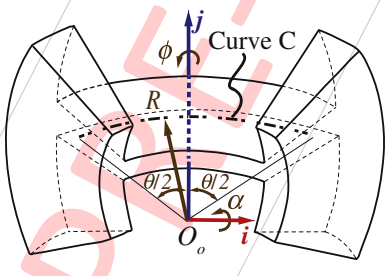

Fig. 3. Spherical flexures.

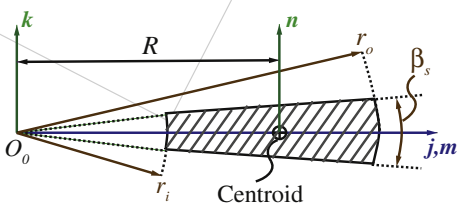

Fig. 4. Cross section properties of SFs.

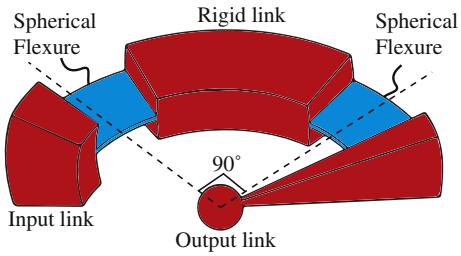

Fig. 5. 2R compliant chain.

with rectangular cross-section to devise a spherical Young parallel mechanism. Apart the works by Lobontiu et al. and that by Li and Chen, all the aforementioned studies are based on the use and proper combination of primitive flexures that are specifically conceived for prevalent planar motions only.

This paper analyzes the compliance performances of a flexure that has been specifically conceived for spherical compliant mechanisms. The flexure, hereafter identified as Spherical Flexure or SF in short, features an arc of a circle as a centroidal axis (see curve C in Fig. 3) and an annulus sector as cross section (Fig. 4), with circle and annulus sharing the same center at point O_0.

The axis of the smaller SF central moment of inertia, I_m, passes through the desired center of spherical motion. This makes the SF exhibit a prevalent compliance with respect to rotations occurring about axes lying on the centroidal axis plane. In fact, preliminary investigations previously performed by the authors [23] suggest that the introduction of SFs seems promising in order to reduce parasitic motions in compliant spherical chains such as, for instance, the 2R and 3R spherical chains (Figs. 5 and 6). Owing to these considerations, this paper thoroughly addresses the analytical derivation of the SF compliance matrix as a function of both hinge dimensions and employed material. In particular, each matrix element is computed resorting to the general method proposed by Jafari et al. [24] and accounting for the exact expression of the torsional constant as found in previous literature [25]. After compliance factors' verification via three-dimensional Finite Element Analysis (FEA), the proposed SF is finally compared in terms of parasitic motions to a CCBF featuring equivalent primary compliance with respect to moments acting in the centroidal axis plane.

2. Closed-form compliance equations for Spherical Flexures

2.1. Formulation

Similarly to Ref. [24], referring to Fig. 7, consider a curved cantilever beam with uniform cross section and with a circular centroidal axis that is centered at point O_0. The beam features one fixed end (on the left, at node 1) and is generically loaded at the opposite free end (on the right). For the beam, define a free end coordinate system S_0, with origin in O_0 and orthogonal axes **i**, **j** and **k**, where **j** lies along the intersection between beam symmetry plane and centroidal axis plane, **k** is perpendicular to the centroidal axis plane and **i** follows the right hand rule. In addition, define a local coordinate system S_l located on the centroid of a generic beam cross section and with axes **l**, **m** and **n** lying along the tangent, normal and binormal to the beam centroidal

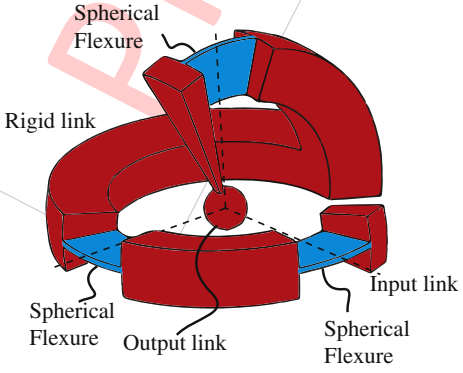

Fig. 6. 3R compliant chain.

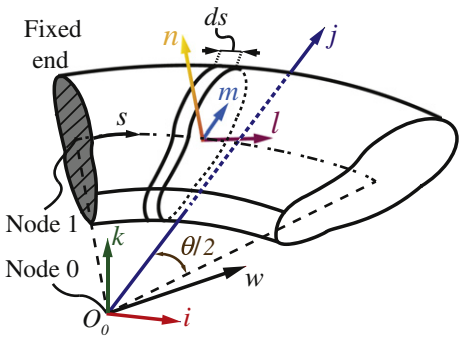

Fig. 7. Generic cantilever curved beam loaded at the free end.

axis (that is, **l**, **m** and **n** are the cross section tangent and principal unit vectors, with **n** being parallel to **k**). As a result of load application, the beam deforms and produces a change in position and orientation of the free end. Let ${}^0\mathbf{w}$ (with components expressed in S_0) describe the external generalized force vector applied at the free end and ${}^0\mathbf{s}$ (with components expressed in S_0) describe the resulting displacement vector of the free end:

$$\begin{aligned} {}^0\mathbf{w} &= [\, f_x \;\; f_y \;\; f_z \;\; m_x \;\; m_y \;\; m_z \,]^T \\ {}^0\mathbf{s} &= [\, u \;\; v \;\; w \;\; \alpha \;\; \phi \;\; \psi \,]^T \end{aligned} \tag{1}$$

The terms f_x, f_y, f_z and m_x, m_y, m_z denote, respectively, the three forces and torques applied to the beam free end, whereas u, v, w and α, ϕ, ψ denote, respectively, the three displacements and rotations undergone by the beam free end along the **i**, **j** and **k** directions. Applied forces are considered to pass through point O_0; displacements are those of point O_0 that moves rigidly with the flexure free end.

The curve defining the centroidal axis (i.e. the circular curve C with center O_0 in Figs. 1 and 3) is described by means of vector ${}^0\mathbf{r}(s)$, namely the position vector connecting the centroid of the section to the center of S_0, the variable s being the curvilinear coordinate along curve C. The relative orientation of the local and global coordinates can be expressed by means of the rotation matrix ${}^l\mathbf{R}_0(s)$, so that ${}^l\mathbf{R}_0(s) = [\,\mathbf{l}\;\mathbf{m}\;\mathbf{n}\,]^T \cdot [\,\mathbf{i}\;\mathbf{j}\;\mathbf{k}\,]$.

The load ${}^0\mathbf{w}$ acting on the free end is balanced by a load ${}^l\mathbf{w}'$ acting on the element ds. This load ${}^l\mathbf{w}'$ produces a deformation per unit length, ${}^l\mathbf{E}$, on the same element. The vectors ${}^l\mathbf{w}'$ and ${}^l\mathbf{E}$ and the corresponding analytical relation can be expressed as:

$$\begin{aligned} {}^l\mathbf{w}' &= [\, f_l \;\; f_m \;\; f_n \;\; m_l \;\; m_m \;\; m_n \,]^T \\ {}^l\mathbf{E} &= [\, \epsilon_{ll} \;\; \gamma_{lm} \;\; \gamma_{ln} \;\; \kappa_{ll} \;\; \kappa_{lm} \;\; \kappa_{ln} \,]^T \\ {}^l\mathbf{w}' &= \mathbf{K} \cdot {}^l\mathbf{E} \end{aligned} \tag{2}$$

The terms f_l, f_m, f_n and m_l, m_m, m_n denote, respectively, the three forces and torques applied to the element ds, whereas ϵ_{ll}, γ_{lm}, γ_{ln} and κ_{ll}, κ_{lm}, κ_{ln} denote, respectively, the three displacements and rotations undergone by the element ds along the **l**, **m** and **n** directions. In addition, the matrix **K** is the rigidity matrix of the element ds that can be written as:

$$\mathbf{K} = \begin{bmatrix} EA & 0 & 0 & 0 & 0 & 0 \\ 0 & b_m GA & 0 & 0 & 0 & 0 \\ 0 & 0 & b_n GA & 0 & 0 & 0 \\ 0 & 0 & 0 & GJ & 0 & 0 \\ 0 & 0 & 0 & 0 & EI_m & 0 \\ 0 & 0 & 0 & 0 & 0 & EI_n \end{bmatrix} \tag{3}$$

where A, b_m, b_n, I_m, I_n, J, E and G are, respectively, cross section area, shear coefficients, area moments of inertia and torsional constant of the beam's cross section, Young's modulus and shear modulus of the employed material. The deformation, $d^l\mathbf{s}'$, of the element ds, due to the load ${}^l\mathbf{w}'$, is defined by:

$$d^l\mathbf{s}' = [\, du' \;\; dv' \;\; dw' \;\; d\alpha' \;\; d\phi' \;\; d\psi' \,]^T = {}^l\mathbf{E} \cdot ds \tag{4}$$

where u', v', w' and α', ϕ', ψ' are respectively displacements and rotations of the element ds in the **l**, **m** and **n** directions. The load ${}^l\mathbf{w}'$, acting on ds and due to the presence of a load ${}^0\mathbf{w}$ on the free end, can be computed via the adjoint transformation matrix

${}^{l}\mathbf{T}_0$ between free end and local coordinates. In particular, the following relation holds:

$$ {}^{l}\mathbf{w}' = {}^{l}\mathbf{T}_0 \cdot {}^{0}\mathbf{w}, \quad \text{where} \quad {}^{l}\mathbf{T}_0 = \begin{bmatrix} {}^{l}\mathbf{R}_0 & \mathbf{0} \\ {}^{l}\mathbf{R}_0 \cdot {}^{0}\tilde{\mathbf{r}}^{T} & {}^{l}\mathbf{R}_0 \end{bmatrix} \tag{5} $$

having defined ${}^{0}\tilde{\mathbf{r}}_s$ as the cross product matrix of vector ${}^{0}\mathbf{r}$. In addition, the deformation of the element ds, denoted as $d^{l}\mathbf{s}'$, causes a deformation at the free end, $d^{0}\mathbf{s}$, that can be calculated by merging Eqs. (2), (4), and (5) as:

$$ d^{0}\mathbf{s} = {}^{l}\mathbf{T}_0^{T} \cdot d^{l}\mathbf{s}' \quad \Rightarrow \quad d^{0}\mathbf{s} = {}^{l}\mathbf{T}_0^{T} \cdot \mathbf{K}^{-1} \cdot {}^{l}\mathbf{T}_0 \cdot {}^{0}\mathbf{w} \cdot ds \tag{6} $$

By integrating Eq. (6) along curve C, one can find the relation between the load ${}^{0}\mathbf{w}$ and the displacement ${}^{0}\mathbf{s}$ of the free end as follows:

$$ {}^{0}\mathbf{s} = {}^{0}\mathbf{C} \cdot {}^{0}\mathbf{w}, \quad \text{where} \quad {}^{0}\mathbf{C} = \int_C {}^{l}\mathbf{T}_0^{T} \cdot \mathbf{K}^{-1} \cdot {}^{l}\mathbf{T}_0 \cdot ds \tag{7} $$

Matrix ${}^{0}\mathbf{C}$ is the compliance matrix for a general cantilever curved beam loaded at the free end and represents the relationship between the applied loads and the corresponding deflections at the same point O_o. For a generic circular beam, the following expressions are found concerning vector ${}^{0}\mathbf{r}$, matrix ${}^{l}\mathbf{R}_0$ and, therefore, for matrix ${}^{l}\mathbf{T}_0$:

$$ {}^{0}\mathbf{r} = \begin{bmatrix} -R\sin(\theta) \\ R\cos(\theta) \\ 0 \end{bmatrix} \quad {}^{l}\mathbf{R}_0 = \begin{bmatrix} \cos(\theta) & \sin(\theta) & 0 \\ -\sin(\theta) & \cos(\theta) & 0 \\ 0 & 0 & 1 \end{bmatrix} \quad {}^{l}\mathbf{T}_0 = \begin{bmatrix} \cos(\theta) & \sin(\theta) & 0 & 0 & 0 & 0 \\ -\sin(\theta) & \cos(\theta) & 0 & 0 & 0 & 0 \\ 0 & 0 & 1 & 0 & 0 & 0 \\ 0 & 0 & -R & \cos(\theta) & \sin(\theta) & 0 \\ 0 & 0 & 0 & -\sin(\theta) & \cos(\theta) & 0 \\ R\cos(\theta) & R\sin(\theta) & 0 & 0 & 0 & 1 \end{bmatrix} \tag{8} $$

The variable R and θ in Eq. (8) represent the radius and subtended angle of the centroidal axis as depicted in Figs. 1 and 3. By inserting the expression for ${}^{l}\mathbf{T}_0$ in Eq. (7), the compliance matrix, ${}^{0}\mathbf{C}$, of a circular beam with uniform cross section (see, e.g. Fig. 7) can be computed as follows:

$$ {}^{0}\mathbf{C} = \begin{bmatrix} C_{x,f_x} & 0 & 0 & 0 & 0 & C_{x,m_z} \\ 0 & C_{y,f_y} & 0 & 0 & 0 & 0 \\ 0 & 0 & C_{z,f_z} & C_{z,m_x} & 0 & 0 \\ 0 & 0 & C_{\theta_x,f_z} & C_{\theta_x,m_x} & 0 & 0 \\ 0 & 0 & 0 & 0 & C_{\theta_y,m_y} & 0 \\ C_{\theta_z,f_x} & 0 & 0 & 0 & 0 & C_{\theta_z,m_z} \end{bmatrix} \tag{9} $$

where:

$$ \begin{aligned} C_{x,f_x} &= \frac{R\left(Ab_mGR^2(\theta+\sin(\theta)) + I_n(\theta(b_mG+E) + (b_mG-E)\sin(\theta))\right)}{2EAb_mGI_n} & C_{y,f_y} &= -\frac{R\left(Ab_mGR^2(\sin(\theta)-\theta) - I_n(\theta(b_mG+E) + (E-b_mG)\sin(\theta))\right)}{2EAb_mGI_n} \\ C_{x,m_z} &= C_{\theta_z,f_x} = \frac{2R^2\sin(\theta/2)}{EI_n} & C_{z,f_z} &= \frac{\theta R\left(Ab_nR^2 + J\right)}{Ab_nGJ} \\ C_{z,m_x} &= C_{\theta_x,f_z} = \frac{-2R^2\sin(\theta/2)}{GJ} & C_{\theta_x,m_x} &= \frac{R\left(GJ(\theta-\sin(\theta)) + EI_m(\theta+\sin(\theta))\right)}{2EGJI_m} \\ C_{\theta_y,m_y} &= -\frac{R\left(E(\sin(\theta)-\theta)I_m - GJ(\theta+\sin(\theta))\right)}{2EGJI_m} & C_{\theta_z,m_z} &= \frac{R\theta}{EI_n} \end{aligned} \tag{10} $$

In case the flexure can be reasonably approximated as a slender beam (i.e. the length to thickness ratio is ≥10, as suggested in Ref. [26]), shear induced deformations become negligible and the shear coefficients, b_m and b_n in Eq. (3), can be set to infinity. With this position, the compliance factors C_{x,f_x}, C_{y,f_y}, and C_{z,f_z} simplify as follows:

$$ C_{x,f_x} = \frac{R\left((\theta+\sin(\theta))\left(AR^2+I_n\right)\right)}{2EAI_n} \qquad C_{y,f_y} = -\frac{R\left((\sin(\theta)-\theta)\left(AR^2+I_n\right)\right)}{2EAI_n} \qquad C_{z,f_z} = \frac{R^3\theta}{GJ} \tag{11} $$

Equations (9)–(11) hold for any slender circularly curved beam with generic cross section and undergoing small deflections around its undeformed configuration. As such, they can be specialized for slender SFs and CCBFs on the basis of the specific expressions for the flexure characteristic parameters A, J, I_m and I_n. Irrespective of the beam cross section, Eq. (9) shows that

the purely translational and rotational sub-blocks of matrix ${}^0\mathbf{C}$ are diagonal, which means that axes **i**, **j** and **k** are aligned to the principal directions of compliance of the flexure. However, for the chosen origin of S_0, some coupling exists between the rotational and translational components of loading and deflection. In particular, moments applied about the **i** and **k** axes induce displacements along **k** and **i** directions respectively (and of course, due to matrix symmetry, forces applied along the **i** and **k** axes induce rotations about **k** and **i** directions respectively). This means that point O_0 is not the elastic center of the hinge (also referred to as center of stiffness [27]). Moreover, the following is worth to be mentioned: like the CCBF, despite its spherical geometry, also the SF does not guarantee a perfect spherical motion of its free end. Indeed, non-zero forces (f_x, f_y, and f_z) and torques (m_z and m_x) about **k** and **i** directions produce undesired non-zero displacements of point O_0. Nonetheless, Eqs. (9)–(11) highlight that a nearly spherical motion for the free end of circularly curved beams can be accomplished by selecting hinge cross sections with large ratios J/I_m and I_n/I_m, and with relatively large area A. In such an instance, indeed, only the primary compliance factors C_{θ_x,m_x} and C_{θ_y,m_y} remain of finite value, whereas all the secondary compliance factors C_{x,f_x}, C_{y,f_y}, C_{z,f_z}, C_{x,m_z}, C_{z,m_x} and C_{θ_z,m_z} tend to vanish. By exploiting this, in the following, the annulus sector cross section of the SF is shown to outperform the rectangular cross section of an equivalent CCBF in providing a flexure with free end deflections that are closer to spherical motions (that is, a flexure with smaller secondary compliance factors).

2.2. Cross section properties and torsional constant

In order to compute the SF and CCBF compliance matrices as a function of the hinge geometry, it is necessary to analytically express the cross sectional properties in terms of the flexure dimensions. Concerning the SF cross section, it features an annulus sector as depicted in Fig. 4, which can be considered as the common section of two concentric circular sectors with different radii. Let one define r_i and r_o as the radii of the inner and outer circular sectors respectively. Assuming β_s as the subtended angle of the annulus sector, the cross section area, A^S can be simply computed as follows:

$$A^S = \frac{r_o^2\beta_s}{2} - \frac{r_i^2\beta_s}{2} = \frac{(r_o^2 - r_i^2)\beta_s}{2} \tag{12}$$

In addition, a relation between the radius of the centroidal axis, R, and the cross section geometric variables r_i, r_o, and β_s, can be found resorting to the definition of the first moment of area, S_k^S, along the **k** axis, such that:

$$S_k^S = A^S R = \int_{-\beta_s/2}^{\beta_s/2}\int_{r_i}^{r_o} (r\cos\beta) r\, dr\, d\beta = \frac{2}{3}(r_o^3 - r_i^3)\sin\beta_s/2 \Rightarrow R = S_k^S/A^S = \frac{4}{3}\frac{(r_o^3 - r_i^3)\sin\beta_s/2}{(r_o^2 - r_i^2)\beta_s} \tag{13}$$

having defined r as the radius of the generic circular sector. The area moments of inertia, I_m^S and I_n^S, with respect to the **m** and **n** axes (see Fig. 4) can then be written as:

$$I_m^S = \int_{-\beta_s/2}^{\beta_s/2}\int_{r_i}^{r_o} (r\sin\beta)^2 r\, dr\, d\beta = \frac{1}{8}(r_o^4 - r_i^4)(\beta_s - \sin\beta_s) \tag{14}$$

$$I_n^S = \int_{-\beta_s/2}^{\beta_s/2}\int_{r_i}^{r_o} (r\cos\beta)^2 r\, dr\, d\beta - A^S R^2 = \frac{1}{8}(r_o^4 - r_i^4)(\beta_s + \sin\beta_s) - \frac{8}{9}\frac{(r_o^3 - r_i^3)^2\sin^2(\beta_s/2)}{(r_o^2 - r_i^2)\beta_s} \tag{15}$$

Note that, in Eq. (15), the term $A^S R^2$ (the area A^S being expressed via Eq. (12)) arises from the use of the parallel axis theorem [28] when transferring the area moment of inertia from the global **k** axis to the local **n** axis.

For what concerns the SF torsional constant, J^S, non-circular cross sections tend to warp when subjected to torsional loading, thus loosing their initial in-plane configuration. The process of formulating an analytical expression (the so-called warping function), which suitably captures this phenomenon, is widely known as the Saint-Venant's torsion problem [29]. Since no closed-form solutions for several types of cross sections are available [30], various techniques to express reliable warping functions have been investigated in the past literature. For instance, Prandtl has introduced membrane analogy [31], which has been proven as a valuable tool for solving the torsion problem for various cross sections (such as rectangular ones). As for the torsional constant, J^S, the exact formulation for annulus sectors is reported in Ref. [32], which proposed a warping function composed of an infinite series of analytical terms. Nevertheless, the authors of Refs. [25,32] recall the following simplified closed-form equation, firstly proposed by J. B. Reynolds, which is in close agreement with the original formulation:

$$J^S = \frac{(r_o - r_i)}{12}(t_o + t_i)(t_o^2 + t_i^2) - V_L t_o^4 - V_S t_i^4 \tag{16}$$

where:

$$V_L = 0.10504 - 0.1\mu + 0.0848\mu^2 - 0.06746\mu^3 + 0.05153\mu^4 \tag{17}$$
$$V_S = 0.10504 + 0.1\mu + 0.0848\mu^2 + 0.06746\mu^3 + 0.05153\mu^4$$
$$\mu = \frac{t_o - t_i}{r_o - r_i}$$

The terms t_o and t_i in Eq. (16) are defined as the chord lengths for the outer and inner sectors respectively. By replacing Eqs. (12), (14), (15) and (16) in Eq. (9), the SF compliance matrix is determined as a function of the hinge geometric parameters and employed material.

For what concerns the CCBF, it simply features a rectangular shape cross section, whose area, A^C, and area moments of inertia, I_m^C and I_n^C, can be trivially computed as:

$$A^C = wt \qquad I_m^C = \frac{1}{12}\, wt^3 \qquad I_n^C = \frac{1}{12}\, tw^3 \tag{18}$$

where, with reference to Fig. 2, w and t are the hinge thickness and width respectively.

As regards the CCBF torsional constant, a comprehensive description of the membrane analogy procedure [31] for rectangular cross sections can be found in Ref. [33], which also shows that for narrow rectangular sections with large w/t ratio, the following simplified closed-form equation holds with a resulting error not greater than 4%:

$$J^C = wt^3\left(\frac{1}{3} - 0.21\frac{t}{w}\left(1 - \frac{t^4}{12w^4}\right)\right) \tag{19}$$

By replacing Eqs. (18) and (19) in Eq. (9), the CCBF compliance matrix is determined as a function of the hinge geometric parameters and employed material.

3. Numerical example and model validation

3.1. Characterization of Spherical Flexures and Finite Element Analysis

The analytical expressions (Eqs. (9)–(11)) for the compliance factors that have been obtained in the previous section are valid for slender beams (that is, with $w^* = \frac{r_o - r_i}{R} < \theta/10$ and $\beta_s < \theta/10$) and for small deflections about the undeformed configuration. First, the accuracy of these expressions has been verified through three dimensional (3D) Finite Element Analysis (FEA) for two different SF geometries with cross-section dimensions respectively well within and very close to the slender-beam approximation limits. Specifically, the fist SF features $r_i = 110$ mm, $r_o = 115$ mm, $\beta_s = \pi/180$, $\theta = \pi/6$ (that is, $w^* = \theta/11.77$ and $\beta_s = \theta/30$); the second SF features $r_i = 110$ mm, $r_o = 128$ mm, $\beta_s = 0.135$, $\theta = \pi/2$ (that is, $w^* = \theta/10.4$ and $\beta_s = \theta/11.63$). Both flexures are made with an Acrylic Plastic with Young's modulus $E = 3000$ MPa and Poisson's ratio $\nu = 0.33$. FEA has been conducted in COMSOL using the Solid Stress–Strain application mode of the Structural Mechanics Module. The global displacements in the **i**, **j** and **k** directions are the degrees of freedom (dependent variables) in this application mode. Linear Elastic Material Model accounting large deformations is chosen. The 3D solid model of the hinge is discretized using the automatic meshing routine available in the software. The resulting meshes for the first and second SFs respectively consist of 10024 and 20029 tetrahedral elements and 16170 and 29734 nodes. FEA simulations are executed by individually loading the flexures along the **i**, **j** and **k** axes and by solving for the corresponding free end deflections. Consistent with the small deflection hypothesis that is at the basis of the analytical model, the magnitude of the loads has been selected so as to limit flexure maximum deformation to less than 0.66%. The compliance factors are then computed as the ratios between each applied force or torque and the corresponding hinge free end displacements and rotations. Comparison between analytically and FEA derived compliance factors is shown in Tables 1 and 2 which show a good match with maximum errors within 2.9% and 8.4% respectively for the first SF and the second considered SF. The higher error resulting for the second case is expected since this SF is stockier than the first one.

After FEA validation, the analytical model has then been used to estimate the components of the SF compliance matrix for various beam lengths obtained via different combinations of centroidal axis radius R and subtended angle θ. The different values of R are obtained by fixing r_i ($r_i = 110$ mm) and varying r_o from 112 mm to 115 mm. The angle θ is chosen in the range of 0.5 rad and 1.5 rad. The other cross section parameter is taken as $\beta_s = \pi/180$. The material considered for the hinge is the same Acrylic Plastic mentioned above. The results are shown in Figs. 8a–8h, which highlight that all the factors increase in absolute value as the centroidal axis length decreases and the subtended angle increases.

3.2. Quantitative comparison between Spherical Flexures and Circularly Curved-Beam Flexures

In order to evaluate the suitability of the SF to generate nearly spherical free end motions for application in spherical mechanisms, its compliance behavior is here compared to that of an equivalent CCBF having identical centroidal axis and subtended

Table 1
Compliance factors for the first slender SF and comparison between analytical and FEA results.

Compliance factors	$C_{x,f_x}[mN^{-1}]$	$C_{x,m_z}=C_{\theta_z,f_x}[N^{-1}]$	$C_{y,f_y}[mN^{-1}]$	$C_{z,f_z}[mN^{-1}]$
Analytic	0.0119	0.1068	2.7402e−4	0.0697
FEA	0.0118	0.1065	2.7793e−4	0.0676
Error (%)	0.8	0.3	1.4	2.9
Compliance factors	$C_{\theta_x,m_x}[m^{-1}N^{-1}]$	$C_{z,m_x}=C_{\theta_x,f_z}[N^{-1}]$	$C_{\theta_y,m_y}[m^{-1}N^{-1}]$	$C_{\theta_z,m_z}[m^{-1}N^{-1}]$
Analytic	5.5181	−0.6120	6.2069	0.9603
FEA	5.3606	−0.5939	6.1699	0.9581
Error (%)	2.8	2.9	0.6	0.2

angle, and exhibiting identical rotational compliance for moments applied along directions orthogonal to that of axis **k**. This last constraint is imposed by equating, for the two different flexure cross sections, the moment of inertia about **m** axis and the torsion constant (namely, $I_m^S = I_m^C$ and $J^S = J^C$, where the subscript *S* and *C* hold for SF and CCBF cases). This has been done since the rectangular cross section is fully characterized by only two independent parameters (namely, w and t) and since C_{θ_x,m_x} and C_{θ_y,m_y} are the largest compliance factors for the considered circularly curved flexures. For the two SFs with the specific geometries considered before, the equivalent CCBFs respectively result with $w = 5$ mm and $t = 2$ mm, and $w = 17$ mm and $t = 16.4$ mm. The resulting analytical compliance factors are reported in Tables 3 and 4 along with the corresponding values computed via FEA. Also for these CCBFs, analytical model and FEA results show good agreement, with maximum errors within 2.9% and 4.9% respectively for the first flexure and the second flexure.

Comparison between Tables 1 and 3, and Tables 2 and 4 highlights that, for the considered hinge dimensions, the considered SFs outperform the equivalent CCBFs since the following compliance ratios

$$r_1 = \frac{C^S_{x,f_x}}{C^C_{x,f_x}} = \frac{C^S_{y,f_y}}{C^C_{y,f_y}} = \frac{A^C I^C_n \left(A^S R^2 + I^S_n\right)}{A^S I^S_n \left(A^C R^2 + I^C_n\right)}$$
$$r_2 = \frac{C^S_{x,m_z}}{C^C_{x,m_z}} = \frac{C^S_{\theta_z,f_x}}{C^C_{\theta_z,f_x}} = \frac{C^S_{\theta_z,m_z}}{C^C_{\theta_z,m_z}} = \frac{I^S_n}{I^C_n} \tag{20}$$

are slightly lower than one, meaning that SFs are less prone than CCBFs to undergo parasitic motions (namely, free end motions that are not spherical). A more comprehensive comparison between SFs and CCBFs should verify the value of these ratios over a rather wide range of choices for flexure length and cross section dimensions.

This is accomplished in Figs. 9a–9f, each reporting for a different value of the flexure subtended angle, the contour plot of the largest value of these ratios ($r = max(r_1, r_2)$) as a function of the dimensionless width w^* and angular span β_s of the SF cross section. In particular, $\theta = 30°, 40°, 50°, 60°, 75°$, and $90°$ is respectively considered in Figs. 9a–9f. In each figure, the considered ranges for w^* and β_s are chosen so as to make the resulting flexure a slender one (that is, with $w^* < \theta/10$ and $\beta_s < \theta/10$) and with I_m lower than I_n (that is C_{θ_z,m_z} lower than C_{θ_x,m_x} and C_{θ_y,m_y}). As shown, for all the considered cross sections, the compliance ratios are always lower than one, which means that the SF always outperforms the CCBF in terms of lower parasitic motions. In particular, irrespective of the value chosen for the angle θ, Figs. 9a–9f highlight that several suitable combinations of w^* and β_s always exist which make the SF 15% stiffer against motions that are not spherical than the equivalent CCBF featuring identical

Table 2
Compliance factors for the second slender SF and comparison between analytical and FEA results.

Compliance factors	$C_{x,f_x}[mN^{-1}]$	$C_{x,m_z}=C_{\theta_z,f_x}[N^{-1}]$	$C_{y,f_y}[mN^{-1}]$	$C_{z,f_z}[mN^{-1}]$
Analytic	9.3269e−5	8.5970e−4	2.0709e−5	2.1667e−4
FEA	9.2310e−5	8.5135e−4	2.0798e−5	1.9997e−4
Error (%)	1.1	1	0.4	7.7
Compliance factors	$C_{\theta_x,m_x}[m^{-1}N^{-1}]$	$C_{z,m_x}=C_{\theta_x,f_z}[N^{-1}]$	$C_{\theta_y,m_y}[m^{-1}N^{-1}]$	$C_{\theta_z,m_z}[m^{-1}N^{-1}]$
Analytic	0.0143	−0.0016	0.0109	0.0080
FEA	0.0131	−0.0015	0.0104	0.0074
Error (%)	8.4	6.1	4.9	7.7

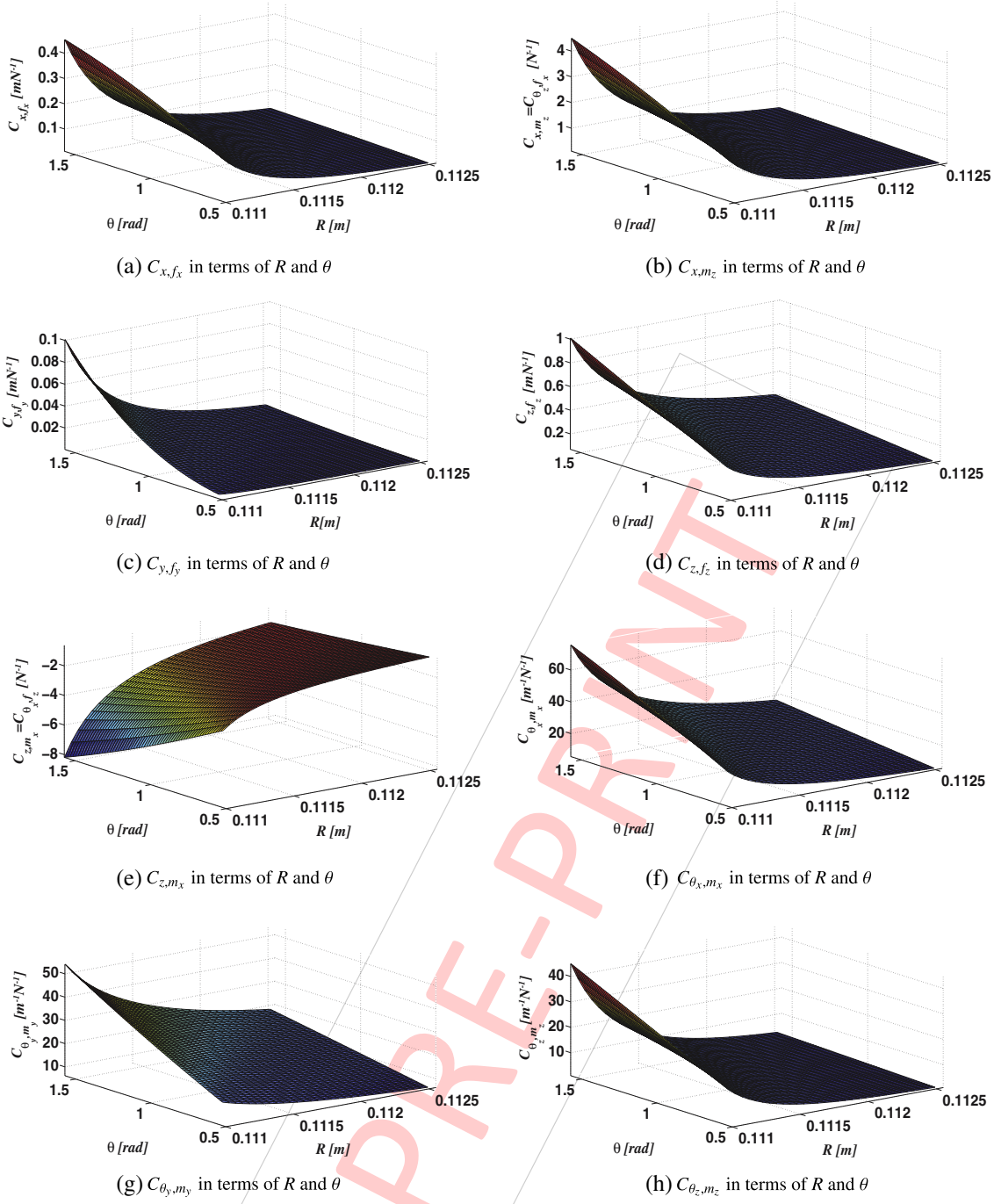

(a) C_{x,f_x} in terms of R and θ

(b) C_{x,m_z} in terms of R and θ

(c) C_{y,f_y} in terms of R and θ

(d) C_{z,f_z} in terms of R and θ

(e) C_{z,m_x} in terms of R and θ

(f) C_{θ_x,m_x} in terms of R and θ

(g) C_{θ_y,m_y} in terms of R and θ

(h) C_{θ_z,m_z} in terms of R and θ

Fig. 8. Compliance factors in terms of R and θ.

primary rotational compliances. This result can be of high importance for slender flexures that need to be designed to provide very precise motions.

3.3. Comparison between non-slender Spherical and Circularly Curved-Beam Flexures

The results reported in Figs. 9a–9f have been computed using the analytical models of SF and CCBF compliances which are only valid within the slender beam approximation limit (that is, $w^* < \theta/10$ and $\beta_s < \theta/10$ for the SF, and $w/R < \theta/10$

Table 3
Compliance factors for the first slender CCBF and comparison between analytical and FEA results.

Compliance factors	$C_{x,f_x}[mN^{-1}]$	$C_{x,m_z}=C_{\theta_z,f_x}[N^{-1}]$	$C_{y,f_y}[mN^{-1}]$	$C_{z,f_z}[mN^{-1}]$
Analytic	0.0120	0.1075	2.7587e−4	0.0697
FEA	0.0119	0.1072	2.7964e−4	0.0676
Error (%)	0.7	0.3	1.4	2.9
Compliance factors	$C_{\theta_x,m_x}[m^{-1}N^{-1}]$	$C_{z,m_x}=C_{\theta_x,f_z}[N^{-1}]$	$C_{\theta_y,m_y}[m^{-1}N^{-1}]$	$C_{\theta_z,m_z}[m^{-1}N^{-1}]$
Analytic	5.5181	−0.6120	6.2069	0.9668
FEA	5.3646	−0.6942	6.1643	0.9646
Error (%)	2.8	2.9	0.7	0.2

and $t/R < \theta/10$ for the CCBF). To assess the validity of the analytical model as well as the advantages of SFs over CCBFs also outside this range, two stocky flexure cases are considered in this section. The first assumes a thick and wide SF characterized by $r_i = 110$ mm, $r_o = 164$ mm, $\beta_s = 0.314$, $\theta = \pi/2$ (that is, with $w^* = \theta/4$ and $\beta_s = \theta/5$). The equivalent CCBF is accordingly characterized by $w = 50.9$ mm and $t = 44.4$ mm. The analytical and FEA calculated compliance factors for the two flexures are shown in Tables 5 and 6. The maximum errors (9.2% for the SF and 9.8% for the equivalent CCBF) still show a close agreement between the Analytical method and FEA. In addition, the largest value, $r = 0.88$, of the FEA evaluated compliance ratios confirms the SF as a better alternative than the equivalent CCBF for the generation of spherical motions. The second case assumes a thin but very wide SF characterized by $r_i = 40$ mm, $r_o = 70$ mm, $\beta_s = \pi/40$, $\theta = \pi/4$ (that is, with $w^* = \theta/1.475$ and $\beta_s = \theta/10$). The equivalent CCBF is accordingly characterized by $w = 25.4$ mm and $t = 4.7$ mm. The analytical and FEA calculated compliance factors for these two flexures are shown in Tables 7 and 8. The very large maximum errors (in the order of 90% for both SF and equivalent CCBF) indicate that the analytical model is not suited to evaluate the compliance factors of these last highly non-slender beam geometries. Nonetheless, by looking at Table 9, which reports the ratios between all the FEA calculated compliance factors of SF to those of the equivalent CCBF, the following can be said: 1) despite highly inaccurate in value, the analytical model can still be used to identify the geometry of the equivalent CCBF that features primary compliances identical to those of the corresponding SF; 2) considering the performance indices r_1 and r_2 defined in Eq. (20), the considered large-width SF outperforms the equivalent CCBF by more than 30%. This last result makes the SF concept even more attractive for many real applications that requires non-slender flexures with large width-to-length ratio (even larger than one), which is usually sought to increase flexure rigidity against torques acting along the directions that are tangent to the flexure centroidal axis.

4. Conclusions

The closed-form compliance equations for slender Spherical Flexures (SFs) undergoing small deflections as a function of both hinge dimensions and employed material have been presented and validated via three dimensional Finite Element Analysis. The compliance model accounts for a suitable closed-form equation, derived from the past literature, and includes the warping phenomenon of non-circular cross sections subjected to torsional loading.

Based on the compliance model, SFs have been fully characterized and the influence of flexure geometric parameters on compliance ratios was analyzed. In addition, SFs have been compared to CCBFs with equivalent primary compliance in terms of their ability to produce free end deflections that resemble as close as possible a spherical motion. Results have shown that SFs always outperform CCBFs in generating lower parasitic motions, which makes them better suited for the implementation of spherical mechanisms with superior motion accuracy.

Table 4
Compliance factors for the second slender CCBF and comparison between analytical and FEA results.

Compliance factors	$C_{x,f_x}[mN^{-1}]$	$C_{x,m_z}=C_{\theta_z,f_x}[N^{-1}]$	$C_{y,f_y}[mN^{-1}]$	$C_{z,f_z}[mN^{-1}]$
Analytic	1.0878e−4	0.0010	2.4152e−5	2.1667e−4
FEA	1.0810e−4	9.9705e−4	2.4287e−5	2.1501e−4
Error (%)	0.6	0.6	0.6	0.8
Compliance factors	$C_{\theta_x,m_x}[m^{-1}N^{-1}]$	$C_{z,m_x}=C_{\theta_x,f_z}[N^{-1}]$	$C_{\theta_y,m_y}[m^{-1}N^{-1}]$	$C_{\theta_z,m_z}[m^{-1}N^{-1}]$
Analytic	0.0143	−0.0016	0.0109	0.0093
FEA	0.0140	−0.0016	0.0104	0.0090
Error (%)	2.1	2.3	4.9	3.7

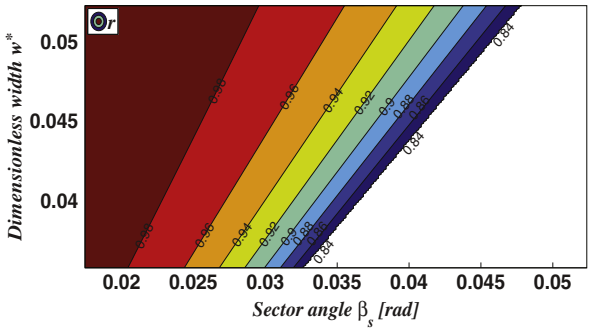

(a) Contour plot of the factor r for $\theta = 30°$

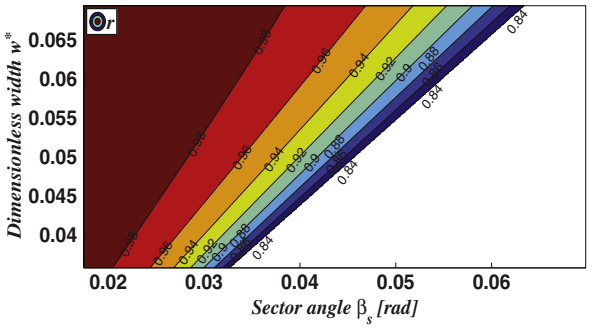

(b) Contour plot of the factor r for $\theta = 40°$

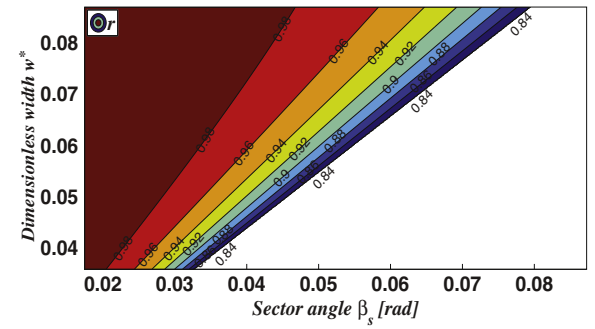

(c) Contour plot of the factor r for $\theta = 50°$

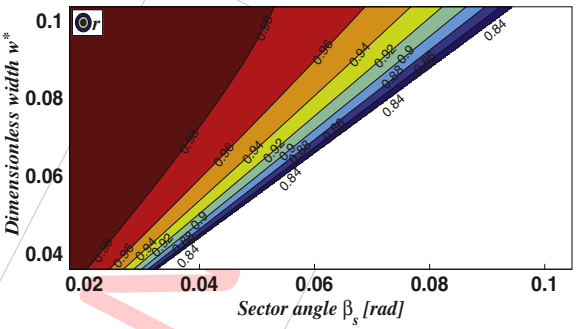

(d) Contour plot of the factor r for $\theta = 60°$

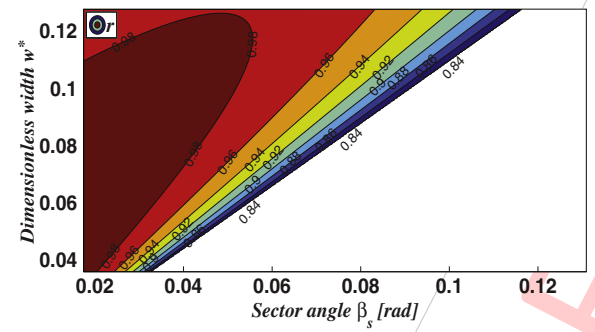

(e) Contour plot of the factor r for $\theta = 75°$

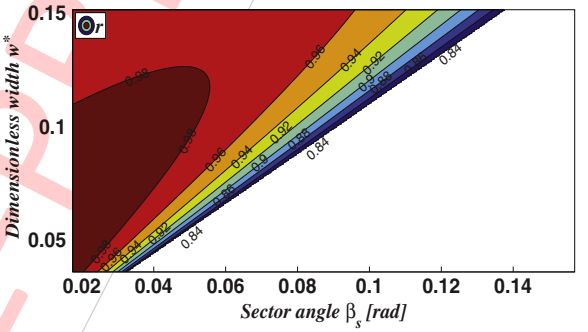

(f) Contour plot of the factor r for $\theta = 90°$

Fig. 9. Contour plots of the factor $r = max(r_1, r_2)$ for different values of θ.

Table 5
Compliance factors for the first non-slender SF and comparison between analytical and FEA results.

Compliance factors	$C_{x,f_x}[mN^{-1}]$	$C_{x,m_z} = C_{\theta_z,f_x}[N^{-1}]$	$C_{y,f_y}[mN^{-1}]$	$C_{z,f_z}[mN^{-1}]$
Analytic	2.0689e−6	1.6267e−5	4.5936e−7	5.1913e−6
FEA	1.9615e−6	1.5514e−5	5.0150e−7	4.7857e−6
Error (%)	5.2	4.6	9.2	7.8
Compliance factors	$C_{\theta_x,m_x}[m^{-1}N^{-1}]$	$C_{z,m_x} = C_{\theta_x,f_z}[N^{-1}]$	$C_{\theta_y,m_y}[m^{-1}N^{-1}]$	$C_{\theta_z,m_z}[m^{-1}N^{-1}]$
Analytic	2.5786e−4	3.3818e−5	2.0905e−4	1.3074e−4
FEA	2.4030e−4	−3.1034e−5	2.0650e−4	1.2310e−4
Error (%)	6.8	8.2	1.2	5.8

Table 6
Compliance factors for the first non-slender CCBF and comparison between analytical and FEA results.

Compliance factors	$C_{x,f_x}[mN^{-1}]$	$C_{x,m_z} = C_{\theta_z,f_x}[N^{-1}]$	$C_{y,f_y}[mN^{-1}]$	$C_{z,f_z}[mN^{-1}]$
Analytic	2.3420e−6	1.8436e−5	5.1999e−7	5.1913e−6
FEA	2.2787e−6	1.8037e−5	5.7124e−7	5.0158e−6
Error (%)	2.7	2.2	9.8	3.4
Compliance factors	$C_{\theta_x,m_x}[m^{-1}N^{-1}]$	$C_{z,m_x} = C_{\theta_x,f_z}[N^{-1}]$	$C_{\theta_y,m_y}[m^{-1}N^{-1}]$	$C_{\theta_z,m_z}[m^{-1}N^{-1}]$
Analytic	2.5786e−4	−3.3818e−5	2.0905e−4	1.4816e−4
FEA	2.4938e−4	−3.2591e−5	2.0218e−4	1.4310e−4
Error (%)	3.3	3.6	3.3	3.4

Table 7
Compliance factors for the second non-slender SF and comparison between analytical and FEA results.

Compliance factors	$C_{x,f_x}[mN^{-1}]$	$C_{x,m_z} = C_{\theta_z,f_x}[N^{-1}]$	$C_{y,f_y}[mN^{-1}]$	$C_{z,f_z}[mN^{-1}]$
Analytic	4.8062e−6	8.5509e−5	2.5212e−7	1.6284e−4
FEA	4.3765e−6	8.0754e−5	5.0150e−7	1.0761e−4
Error (%)	8.9	5.6	98.9	33.9
Compliance factors	$C_{\theta_x,m_x}[m^{-1}N^{-1}]$	$C_{z,m_x} = C_{\theta_x,f_z}[N^{-1}]$	$C_{\theta_y,m_y}[m^{-1}N^{-1}]$	$C_{\theta_z,m_z}[m^{-1}N^{-1}]$
Analytic	0.0521	−0.0028	0.0673	0.0016
FEA	0.0354	−0.0019	0.0650	0.0015
Error (%)	32	32.5	3.5	3.7

Table 8
Compliance factors for the second non-slender CCBF and comparison between analytical and FEA results.

Compliance factors	$C_{x,f_x}[mN^{-1}]$	$C_{x,m_z} = C_{\theta_z,f_x}[N^{-1}]$	$C_{y,f_y}[mN^{-1}]$	$C_{z,f_z}[mN^{-1}]$
Analytic	7.1139e−6	1.2733e−4	3.7317e−7	1.6284e−4
FEA	6.8117e−6	1.2519e−4	7.1981e−7	1.1151e−4
Error (%)	4.2	1.7	92.9	31.5
Compliance factors	$C_{\theta_x,m_x}[m^{-1}N^{-1}]$	$C_{z,m_x} = C_{\theta_x,f_z}[N^{-1}]$	$C_{\theta_y,m_y}[m^{-1}N^{-1}]$	$C_{\theta_z,m_z}[m^{-1}N^{-1}]$
Analytic	0.0521	−0.0028	0.0673	0.0023
FEA	0.0391	−0.0020	0.0622	0.0023
Error (%)	25	30	7.6	0.8

Table 9
Ratio between the SF and equivalent CCBF compliance factors via FEA.

Compliance factors	$C_{x,f_x}[mN^{-1}]$	$C_{x,m_z} = C_{\theta_z,f_x}[N^{-1}]$	$C_{y,f_y}[mN^{-1}]$	$C_{z,f_z}[mN^{-1}]$
Ratio	0.6425	0.6451	0.6967	0.9650
Compliance factors	$C_{\theta_x,m_x}[m^{-1}N^{-1}]$	$C_{z,m_x} = C_{\theta_x,f_z}[N^{-1}]$	$C_{\theta_y,m_y}[m^{-1}N^{-1}]$	$C_{\theta_z,m_z}[m^{-1}N^{-1}]$
Ratio	0.9054	0.9500	1.0450	0.6522

References

[1] Y. Tian, D. Zhang, B. Shirinzadeh, Dynamic modelling of a flexure-based mechanism for ultra-precision grinding operation, Precis. Eng. 35 (4) (2011) 554–565. ISSN 0141-6359.
[2] S. Polit, J. Dong, Development of a high-bandwidth XY nanopositioning stage for high-rate micro-/nanomanufacturing, IEEE/ASME Trans. Mechatron. 16 (4) (2011) 724–733. ISSN 1083-4435.
[3] Y. Moon, J. Choi, A compliant parallel mechanism for needle intervention, 2013 35th Annual International Conference of the IEEE Engineering in Medicine and Biology Society (EMBC), 2013. pp. 4875–4878.
[4] M.B. Hong, Y.-Ho. Jo, Design and evaluation of 2-DOF compliant forceps with force-sensing capability for minimally invasive robot surgery, IEEE Trans. Rob. 28 (4) (2012) 932–941.
[5] N.P. Belfiore, M. Balucani, R. Crescenzi, M. Verotti, Performance analysis of compliant MEMS parallel robots through pseudo-rigid-body model synthesis, ASME ESDA 11th Bienn. Conf. Eng. Syst. Des. Anal. 3 (2012) 329–334.
[6] A. Sauceda-Carvajal, H.D. Kennedy-Cabrera, J. Hernndez-Torres, A.L. Herrera-May, Jos. Mireles, Compliant MEMS mechanism to extend resolution in Fourier transform spectroscopy, Proc. SPIE, Micromachining Microfab. Process Technol. XIX 8973 (2014) 89730S–89730S-9.
[7] J. Paros, How to design flexure hinges, Mach. Des. 37 (1965) 151–156.
[8] N. Lobontiu, J. Paine, E. Garcia, M. Goldfarb, Corner-filleted flexure hinges, J. Mech. Des. 123 (3) (2001) 346–352.
[9] Y. Tian, B. Shirinzadeh, D. Zhang, Y. Zhong, Three flexure hinges for compliant mechanism designs based on dimensionless graph analysis, Precis. Eng. 34 (1) (2010) 92–100.
[10] N. Lobontiu, M. Cullin, In-plane elastic response of two-segment circular-axis symmetric notch flexure hinges: the right circular design, Precis. Eng. 37 (3) (2013) 542–555.
[11] F. Parvari Rad, G. Berselli, R. Vertechy, V. Parenti-Castelli, Evaluating the spatial compliance of circularly curved-beam flexures, Springer, Comput. Kinematics (2013) 329–336.
[12] G. Berselli, F. Parvari Rad, R. Vertechy, V. Parenti Castelli, Comparative evaluation of straight and curved beam flexures for selectively compliant mechanisms, Advanced Intelligent Mechatronics (AIM), 2013 IEEE/ASME International Conference on, IEEE 2013, pp. 1761–1766.
[13] S. Smith, Flexures, Elements of Elastic Mechanisms, Gordon and Breach Science Pub. 2000.
[14] N. Lobontiu, E. Garcia, Two-axis flexure hinges with axially-collocated and symmetric notches, Comput. & Struct. 81 (13) (2003) 1329–1341.
[15] N. Lobontiu, J. Paine, Design of circular cross-section corner-filleted flexure hinges for three-dimensional compliant mechanisms, J. Mech. Des. 124 (3) (2002) 479–484.
[16] B. Trease, Y. Moon, S. Kota, Design of large-displacement compliant joints, J. Mech. Des. 127 (4) (2005) 788–798.
[17] D. Farhadi Machekposhti, N. Tolou, J.L. Herder, The scope for a compliant homokinetic coupling based on review of compliant joints and rigid-body constant velocity universal joints, ASME IDETC, Int. Des. Eng. Tech. Conf. 4 (2012) 379–392.
[18] J. Hesselbach, J. Wrege, A. Raatz, O. Becker, Aspects on design of high precision parallel robots, Assem. Autom. 24 (1) (2004) 49–57.
[19] G. Palmieri, M.C. Palpacelli, M. Callegari, Study of a fully compliant U-joint designed for minirobotics applications, ASME J. Mech. Des. 134 (11) (2012) 111003(9)
[20] J.O. Jacobsen, G. Chen, L.L. Howell, S.P. Magleby, Lamina Emergent Torsional (LET) joint, Mech. and Mach. Theory 44 (11) (2009) 2098–2109.
[21] M. Callegari, A. Cammarata, A. Gabrielli, M. Ruggiu, R. Sinatra, Analysis and design of a spherical micromechanism with flexure hinges, J. Mech. Des. 131 (2009) 051003
[22] G. Li, G. Chen, Achieving compliant spherical linkage designs from compliant planar linkages based on PRBM: a spherical young mechanism case study, Robotics and Biomimetics (ROBIO), 2012 IEEE International Conference on, IEEE, 2012. pp. 193–197.
[23] F. Parvari Rad, G. Berselli, R. Vertechy, V. Parenti Castelli, Stiffness Analysis of a fully compliant spherical chain with two degrees of freedom, Advances in Robot Kinematics, Springer 2014, pp. 273–284.
[24] M. Jafari, M. Mahjoob, An exact three-dimensional beam element with nonuniform cross section, J. Appl. Mech. 77 (6) (2010) 0610091–0610097.
[25] I. Lyse, B. Johnston, Structural beams in torsion, 1934, Fritz Laboratory Reports, 1934.
[26] A. Blake, Handbook of Mechanics, Materials, and Structures, Wiley Series in Mechanical Engineering Practice 1985.
[27] S. Zhang, E.D. Fasse, A finite-element-based method to determine the spatial stiffness properties of a notch hinge, ASME J. Mech. Des. 123 (1) (2001) 141–147.
[28] P. Burton, Kinematics and Dynamics of Planar Machinery, Prentice Hall 1979.
[29] T.J. Higgins, A comprehensive review of Saint-Venant's torsion problem, Am. J. Phys. 10 (5) (1942) 248–259.
[30] W.C. Young, R.G. Budynas, Roark's formulas for stress and strain, 7. McGraw-Hill New York 2002.
[31] T.H.G. Megson, Aircraft Structures for Engineering Students, Elsevier 2012.
[32] A. Love, A Treatise on the Mathematical Theory, Dover Public. 1944.
[33] S. Timoshenko, J. Goodier, Theory of Elasticity, 412. McGraw Hill New York 1951.